Electronic structure of CeAg$_2$Ge$_2$ studied by resonant photoemission spectroscopy

Soma Banik,[1,][*] Aparna Chakrabarti,[1] Devang A. Joshi,[2] A. Thamizhavel,[2] D. M. Phase,[3] S. K. Dhar,[2] and S. K. Deb[1]

[1]*Raja Ramanna Centre for Advanced Technology, Indore 452013, India*
[2]*Tata Institute of Fundamental Research, Homi Bhabha Road, Colaba, Mumbai 400005, India*
[3]*UGC-DAE Consortium for Scientific Research, Khandwa Road, Indore 452001, India*

The electronic structure of CeAg$_2$Ge$_2$ single crystal has been investigated by using valence-band photoemission at different photon energies ranging from 110 to 150 eV. Resonant photoemission has been observed near the 4d threshold of Ce at 121 eV. The constant initial-state spectra shows two photoemission features having 4f character near the Fermi level at −0.4 and −1.7 eV which exhibits Fano-type sharp resonance character. The experimental spectra have been interpreted with the help of calculations based on full-potential linearized augmented plane-wave method using density-functional theory. Excellent agreement has been obtained between the theory and the experiment. The origin of the feature near to Fermi level is related to the Ce 4f states and the feature at −1.7 eV is related to the strong hybridization between the Ce 4f and 5d, Ag 4d and Ge 4p states.

Resonant photoemission spectroscopy (RPES) has emerged as a very powerful tool to understand the electronic states of rare earths. From last few decades, Ce-based inter-metallic compounds have attracted much attention for their various ground-state properties, such as the magnetism, nonmagnetic heavy Fermion, and quantum criticality, etc.[1–6] The diverse ground states are due to the competition between the Ruderman-Kittel-Kasuya-Yosida interaction and the Kondo effect.[7] CeAg$_2$Ge$_2$ belongs to a wide class of cerium compounds that crystallize in the ThCr$_2$Si$_2$ structure having a body-centered tetragonal lattice.[6] At room temperature it exhibits a paramagnetic phase while at low temperature an antiferromagnetic phase with T_N=7 K is reported.[5,6] More recently, detailed studies were performed on a single crystal, which has shown that CeAg$_2$Ge$_2$ orders antiferromagnetically at 4.6 K.[8] The neutron-diffraction experiment shows a sine modulated structure with a magnetic moment equal to 1.85μ_B at T=1.5 K.[6] In the Ce based intermetallic alloys it is believed that the ground-state properties depend on the strength of hybridization of the f electrons with the delocalized band states and this motivated us to understand the electronic structure of CeAg$_2$Ge$_2$. In the present work, we investigate the occupied electronic states of CeAg$_2$Ge$_2$ at room temperature and try to provide a clear understanding of the hybridization between the local Ce 4f electrons and the itinerant conduction electrons by the systematic Ce 4d-4f RPES study.

CeAg$_2$Ge$_2$ single crystal was grown by the self-flux method.[8] For the PE measurements the sample has been mechanically polished to mirror finish using quarter micron diamond paste. The RPES measurements on this sample were carried out at the angle-integrated PE beamline on the Indus-1 synchrotron radiation source.[9] The valence-band (VB) photoemission spectra were recorded using a photon energy of 110–130 eV in very small steps of 1 eV. The energy analyzer from Omicron (EA125) is used to measure the spectra at room temperature. The spectra were normalized by the photon flux estimated from the photocurrent from the post mirror of the beam line. To determine the Fermi edge of the sample we have mounted the sample and the gold foil on the same sample holder, and measured the spectra of gold and the sample one after another at the same monochromator setting. The base pressure in the analysis chamber was 1 $\times 10^{-10}$ mbar. To obtain atomically clean surface the sample has been sputtered with 1.5 keV argon ions and annealed at 500 K. Similar process have been employed to clean the Ni$_2$MnGa single crystals.[10] Surface cleanliness was confirmed by the absence of the O 1s, C 1s, and O 2p signals. The experimental resolution was estimated to be from 0.32 to 0.44 eV in the photon energy range 110–150 eV. For the x-ray photoelectron spectroscopy (XPS) measurement Al $K\alpha$ x-ray source which provides 1486.6 eV photons from Omicron (DAR400) is used. The *ab initio*, relativistic spin-polarized calculations are performed using full-potential linearized augmented plane-wave (FPLAPW) program[11] with the generalized gradient approximation for exchange correlation.[12] An energy cutoff for the plane-wave expansion of about 17 Ry is used ($R_{MT}K_{max}$=9.5). The muffin-tin radii are Ce, 2.6; Ag, 2.5; and Ge, 2.3 a.u. The number of k points for self-consistent field cycles in the reducible (irreducible) Brillouin zone is 8000 (635). The convergence criterion for the total energy E_{tot} is 0.1 mRy. The charge convergence is set to 0.001. The tetrahedron method has been used for k-space integration. The lattice constants are taken from the experiment.[8] Hence the calculations are performed at lattice parameters of a and b=8.127715 and c=20.735973 a.u.

Prior to the RPES measurements the surface composition was estimated from core-level XPS measurements. In Fig. 1 we show the core-level spectra of Ce 3d, Ag 3d and Ge 3d. In order to determine the surface composition, the area under the XPS core-level peaks have been determined by fitting the spectra using a least-square error minimization routine. The core levels have been fitted with Doniac-Šunjić line shape.[13] The inelastic background has been subtracted using Tougaard method.[14] The instrumental broadening is considered by convoluting the line shapes with a Voigt function. The instrumental parameters have been kept fixed during the fitting. For determining composition, we find the atom density (N) for each constituent by normalizing the area under the corresponding core-level peak (I) by the respective photoioniza-
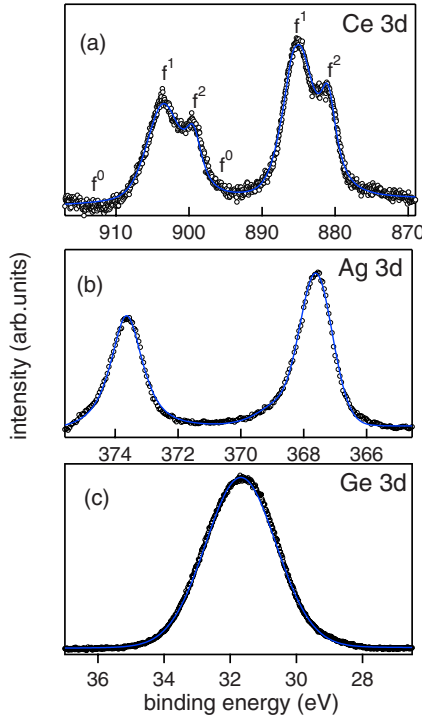
FIG. 1. (Color online) Core-level spectra of $CeAg_2Ge_2$ showing (a) Ce 3d, (b) Ag 3d, and (c) Ge 3d core level. Solid blue line is fit to the experimental data (open circles). In (a) f^n ($n=0,1,2$) designs the final states related to the main peaks of Ce.

FIG. 2. (Color online) Normal emission VB spectra of $CeAg_2Ge_2$ recorded at different photon energy across the 4d-4f resonance. The Fermi edge of gold (red open circle) has been used to align the normalized Fermi edge of the sample (blue solid line) which is shown in the inset for two incident photon energies of 21 and 114 eV.

tion cross section σ,[15] the mean-free path (λ) of the photoelectron for an inorganic compound,[16] and the analyzer étendue given by $G(E) \propto E^{-0.5}$,[17] where E is the kinetic energy of the photoelectron. Thus, $N = \frac{I}{\sigma \cdot \lambda(E) G(E) C}$, where C is a product of the detector efficiency, angular asymmetry photoelectron intensity, flux of the x-ray characteristic line per unit area, inverse cosine of incidence angle, and cosine of emission angle. The surface composition determined in this way is about $Ce_{0.95}Ag_{1.85}Ge_{2.2}$, from the depth of 28 Å, which is the probing depth of the photoelectrons.

From Fig. 1 the $3d_{5/2}$ and $3d_{3/2}$ peak of Ce appears at 885.2 eV and 903.75 eV, respectively, with a spin orbit splitting of 18.4 eV. On the other hand Ag $3d_{5/2}$ and $3d_{3/2}$ appears at 367.8 and 373.8 eV, respectively, with the spin orbit splitting of 6 eV and the Ge 3d peak appears at 31.7 eV. The Ce 3d peak of $CeAg_2Ge_2$ shows two main peaks corresponding to $3d_{5/2}$ and $3d_{3/2}$ spin-orbit component along with the doublets. The main peaks are associated with the poorly screened $3d^9 f^1$ final state. The additional peak labeled as f^2 represents the Ce atoms in the $3d^9 f^2$ state. f^2 peak indicates hybridization of the 4f levels with the other orbitals. f^0 peak arises from the 4+ valence state of Ce. The intensity of f^0 peak in the core level (Fig. 1) is almost negligible which indicates that Ce exists in trivalent state in this compound similar to CeSe.[18] In addition to the f^1 peak, f^0 and f^2 peaks have been observed for other Ce based intermetallic compounds like CeAlCu, CeNi$_2$Si$_2$, CeAlNi, CePd$_3$, and CeNi$_5$B.[18–20]

The VB spectra of $CeAg_2Ge_2$ recorded at different photon energies over 110–150 eV are shown in Fig. 2. The background obtained by the Tougaard procedure[14] has been subtracted from each raw data. The Fermi level of the sample was aligned with respect to the VB spectra of the *in situ* cleaned gold foil at the same monochromator setting and is shown in the inset of Fig. 2 at 21 and at 114 eV incident photon energies. The Fermi edge is not clearly visible mainly due to the poor resolution (≈ 0.4 eV). The VB shows mainly four features marked as A, B, C, and D at -0.4 eV, -1.7 eV, -5.5 eV, and -9.9 eV, respectively. Features A and B are resonantly enhanced above the Ce 4d threshold located around 121 eV in $CeAg_2Ge_2$ and is related to Ce 4f states. This is clearly seen in Fig. 2. The 4d-4f resonance in Ce compounds occurs at photon energies at which 4d core electrons are excited to the 4f states. Ce shows resonance phenomenon particularly due to highly localized excitations of the form $4d^{10}4f^n \rightarrow 4d^{10}4f^{n-1}$, which may decay either by a direct photoemission phenomena: $4d^{10}4f^n + h\nu \rightarrow 4d^{10}4f^{n-1} + e$, or by photoionization of the excited electron into the conduction band followed by Auger emission: $4d^{10}4f^n + h\nu \rightarrow 4d^9 4f^{n+1} \rightarrow 4d^{10}4f^{n-1} + e$. The final states of the two channels are indistinguishable so that there is a quantum interference between the two channels. On closely looking at Fig. 2, two resonance features are observed when photon energies are varied from 110 to 150 eV. The enhanced resonance feature at 121 eV is due to the $4d_{3/2}$ and is much more significant than the one at 111 eV that is mainly due to the $4d_{5/2}$ threshold.[21] From high-resolution photoemission using He resonance lines, Patthey *et al.*,[22] studied the Ce 4f contribution to the photoelectron spectra. The specific aspect of the 4f spectra of Ce compounds is the two-peak profile. One peak occurs at the Fermi edge and the other between 2 and 3 eV below it. Many theoretical works based on the single impurity Anderson model have been reported to explain the
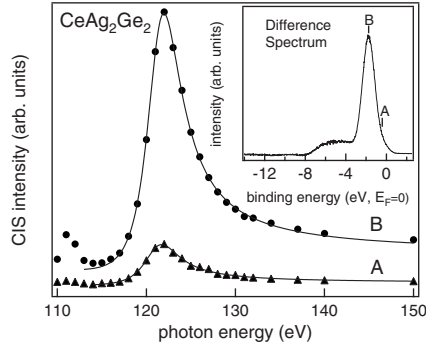
FIG. 3. The constant initial state of the resonant features A and B as a function of photon energy. The solid line shows the fitting with the Fano line shape. Inset shows the difference of the on-resonance spectrum at 121 eV and the off-resonance spectrum at 116 eV.

FIG. 4. (Color online) For $CeAg_2Ge_2$ (a) Total DOS along with the Ce, Ag, and Ge total DOS, (b) partial DOS showing Ce 3d, Ce 4f, Ag 4d, and Ge 4p states, and (c) calculated and experimental valence band (at 118 eV).

two peak profile of the Ce 4f spectra in Ce-based intermetallics such as CeNiSn, $CeFe_2$.[23] Here the second feature related to Ce 4f state is found to be broad and shifted toward the lower binding energy which may be due to the hybridization of the Ce 4f states with the Ag 4d and Ge 4p states.

To evaluate the resonance energy we have plotted the difference spectrum in the inset of Fig. 3 obtained by subtracting the off-resonance VB spectra at an excitation energy of 116 eV from the on-resonance VB spectra at an excitation energy of 121 eV. It is evident in the figure that mainly the features A and B shows the resonant behavior, on the other hand, the features C and D shows a broad peak which does not show a characteristic resonance-type behavior. Hence the constant initial state (CIS) intensity have been plotted only for the features A and B and are shown in Fig. 3. The CIS intensity plots are obtained from Fig. 2 by plotting the normalized intensity of the marked regions (A and B) at fixed binding energy positions of the respective features. A maximum in the intensity of these spectra around a photon energy of 111 and 121 eV is observed. CIS spectra has been shown to give rise to a characteristic line profile for the cross-section variation in the vicinity of the resonance. Fano[24] predicts a line shape for this type of process which obeys the equation: $\sigma(h\nu) = \sigma_a \frac{(q+\epsilon)^2}{1+\epsilon^2} + \sigma_b$, where $\epsilon = (h\nu - E_0)/\Gamma$, E_0 is the resonance energy, Γ is the half-width of the line, and q is the line profile index. The cross sections σ_a and σ_b correspond to the transitions to states of the continuum those, respectively, do and do not interact with the discrete autoionizing state. In Fig. 3 the markers (filled circles and triangles) and the solid line show the experimental data points and the fitted Fano line shape, respectively, achieved with a curve of the form $(q+\epsilon)^2/(1+\epsilon^2)$ for the parameter values q =2.45($\pm$0.06), Γ=4.23($\pm$0.2), and E_0=121.14($\pm$0.06) for feature A and q=2.36($\pm$0.04), Γ=3.995($\pm$0.1), and E_0 =121.38($\pm$0.03) for feature B. The empirical parameters Γ and q are related to the Coulomb potential and the dipole matrix elements. We have not calculated the Coulomb potential and the dipole matrix elements but the determined Γ and q values appear to be reasonable when compared to the values previously reported for other Ce based compounds such as CeNi and Ce-Co.[25,26]
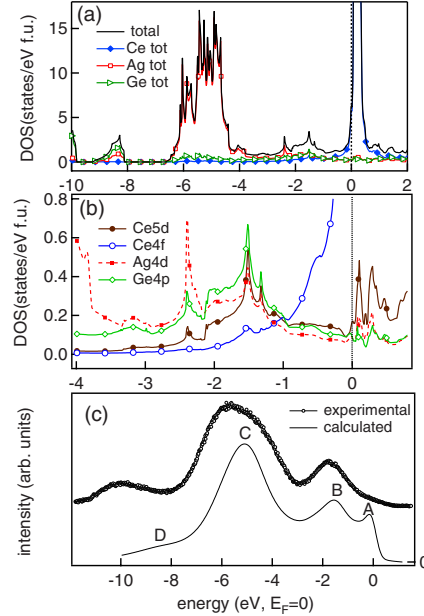
To understand the origin of the features in the experimental VB spectra we show the total density of states (DOS) along with the total Ce, Ag, and Ge DOS in Fig. 4(a). The partial DOS of Ce 5d, Ce 4f, Ag 4d, and Ge 4p states close to the Fermi level from -4 to 1 eV are shown in Fig. 4(b). It is evident from Figs. 4(a) and 4(b) that the DOS of $CeAg_2Ge_2$ near to the E_F are mainly due to the Ce 4f states which extends upto -2 eV. On the other hand a strong hybridization between the Ce, Ag, and Ge states are observed for the features existing at -1.5 and -2.3 eV. The broad feature centering around -5.5 eV is dominated by the Ag 4d states. The feature around -8 eV is due to the hybridization between the Ag and Ge states. Hence it is clear from the DOS that the resonant features A and B observed in the experiment (Fig. 3) is due to the Ce 4f states and the hybridized Ce 4f states with the Ce 5d, Ag 4d, and Ge 4p states, respectively. Ce 5d states are found to be overlapping with the Ce 4f states and contribute for the carriers near E_F in $CeTe_2$ and $CeNi_2Ge_2$.[27] Hence the resonant character of the feature B is mainly due to the hybridized Ce 4f state.

Information about hybridization between Ce 4f orbitals with the other orbitals can be derived from the analysis of Ce 3$d_{5/2}$ core-level peak [Fig. 1(a)].[28] The total hybridization parameter (Δ) is related to the ratio $r = I(f^2)/[I(f^1)+I(f^2)]$, where $I(f^1)$ and $I(f^2)$ are relative intensities of f^1 and f^2 peaks, which in the present case is estimated to be ≈ 0.365. Using a correlation between Δ and r as outlined by Fuggle *et al.*,[28] the value of Δ obtained is ≈ 0.190 eV. For $CeAg_2Ge_2$, Endstra *et al.*,[29] reported the value of hybridization matrix element (V_{df}) between Ce f states and Ag d states calculated using Harrison-Straub model. If we consider that the total hybridization has similar contributions from Ag d states and Ge p states then the value of V_{df} can be approximately calculated from the equation $\Delta_{df} = 2V_{df}^2/B_d$, where B_d is the full

width at half maximum (FWHM) of the Ag d bands (1.2 eV) and $\Delta \approx 2\Delta_{df}$.[28] Hence, the value of V_{df} is estimated to be 0.238 eV which agrees reasonably well with the value of V_{df} reported in Ref. [29].

For comparing the experimental VB with the theory, in Fig. 4(c) we show the DOS which has been broadened by adding the total DOS of Ce, Ag, and Ge. This added DOS is multiplied with the Fermi function at the measurement temperature and convoluted with a Voigt function. The FWHM of the Gaussian component is taken to be 0.4 eV of the Voigt function which represents the instrumental resolution in different measurements. The energy-dependent Lorentzian FWHM that represents the lifetime broadening is $0.3E$, where E is the energy with respect to E_F.[30] The inelastic background and the matrix elements are not considered. This is a standard procedure of comparing the photoemission spectrum with the calculated DOS.[30,31] The features A, B, C, and D obtained from the calculated VB are in very good agreement with the experiment. There are small differences which could be related to the fact that the FPLAPW method is based on density-functional theory (DFT) that is a ground-state calculation and the electron-electron interaction is considered in an average way. The difference between the experiment and DFT can be quantified in terms of self-energy,

where the real part gives the energy shift and the imaginary part gives the broadening. However, sample related effects such as the presence of antisite defects and site disorder that are not considered in the calculation might also be responsible for the small disagreements.[31]

In conclusion, we have studied the electronic structure of $CeAg_2Ge_2$ by using angle-integrated $4d$-$4f$ RPES. The VB spectra show two resonance features A and B observed at -0.4 eV and -1.7 eV, respectively at a 121 eV excitation energy which corresponds to the threshold energy of the Ce $4d$ states. The constant initial state as a function of photon energy shows a good fit with a Fano line-shape profile for the resonance features. From the FPLAPW calculations, the origin of the feature A is related to the Ce $4f$ states and the feature B is related to the strong hybridization between the Ce, Ag, and Ge states. The calculated VB shows an excellent agreement with the experimental spectra.

*soma@rrcat.gov.in

[1] A. H. Castro Neto and B. A. Jones, Phys. Rev. B **62**, 14975 (2000).

[2] E. Bauer, G. Hilscher, H. Michor, C. Paul, E. W. Scheidt, A. Gribanov, Y. Seropegin, H. Noel, M. Sigrist, and P. Rogl, Phys. Rev. Lett. **92**, 027003 (2004).

[3] H. Q. Yuan *et al.*, Science **302**, 2104 (2003).

[4] F. Steglich *et al.*, J. Phys.: Condens. Matter **8**, 9909 (1996).

[5] G. Knopp *et al.*, J. Magn. Magn. Mater. **63-64**, 88 (1987).

[6] A. Loidl, K. Knorr, G. Knopp, A. Krimmel, R. Caspary, A. Bohm, G. Sparn, C. Geibel, F. Steglich, and A. P. Murani, Phys. Rev. B **46**, 9341 (1992).

[7] S. Rahman, T. Mihalisin, J. E. Crow, and P. Schlottmann, Solid State Commun. **75**, 279 (1990).

[8] A. Thamizhavel, R. Kulkarni, and S. K. Dhar, Phys. Rev. B **75**, 144426 (2007).

[9] S. M. Chaudhari, D. M. Phase, A. D. Wadikar, G. S. Ramesh, M. S. Hegde, and B. A. Dassanacharya, Curr. Sci. **82**, 305 (2002).

[10] R. S. Dhaka *et al.*, Surf. Sci. **603**, 1999 (2009).

[11] P. Blaha, K. Schwarz, G. K. H. Madsen, D. Kvasnicka, and J. Luitz, *WIEN2K* (Karlheinz Schwarz, Techn. Universität, Wien, Austria, 2002).

[12] J. P. Perdew, K. Burke, and M. Ernzerhof, Phys. Rev. Lett. **77**, 3865 (1996).

[13] S. Doniach, and M. Šunjić, J. Phys. C **3**, 285 (1970).

[14] S. Tougaard, Surf. Sci. **216**, 343 (1989).

[15] J. J. Yeh and I. Lindau, At. Data Nucl. Data Tables **32**, 1 (1985).

[16] M. P. Seah and W. A. Dench, Surf. Interface Anal. **1**, 2 (1979).

[17] D. Briggs and M. P. Seah, *Practical Surface Analysis, Auger and X-ray Photoelectron Spectroscopy*, 2nd ed. (Wiley, New York, 1990), Vol. 1.

[18] S. Hüfner, *Photoelectron Spectrocopy Principles and Applications* (Springer-Verlag, Berlin, 1995).

[19] R. K. Singhal *et al.*, J. Phys.: Condens. Matter **5**, 4013 (1993).

[20] T. Tolinski, A. Kowalczyk, and G. Chelkowska, Phys. Lett. A **308**, 75 (2003).

[21] A. A. Radzig and B. M. Smirnov, *Reference Data on Atoms, Molecules and Ions* (Springer, Berlin, 1985); A. V. Karol and A. V. Solov'yov, J. Phys. B (to be published).

[22] F. Patthey, B. Delley, W.-D. Schneider, and Y. Baer, Phys. Rev. Lett. **55**, 1518 (1985); F. Patthey, W.-D. Schneider, Y. Baer, and B. Delley, Phys. Rev. B **34**, 2967 (1986).

[23] T. Konishi *et al.*, J. Electron Spectrosc. Relat. Phenom. **88-91**, 411 (1998); **88-91**, 303 (1998).

[24] U. Fano, Phys. Rev. **124**, 1866 (1961).

[25] T. Kashiwakura, S. Suzuki, T. Okane, S. Sato, T. Kinoshita, A. Kakizaki, T. Ishii, Y. Isikawa, H. Yamagami, and A. Hasegawa, Phys. Rev. B **47**, 6885 (1993).

[26] L. Braicovich, C. Carbone, O. Gunnarsson, and G. L. Olcese, Phys. Rev. B **44**, 13756 (1991).

[27] J.-S. Kang *et al.*, J. Phys.: Condens. Matter **16**, 9163 (2004); D. Ehm, F. Reinert, G. Nicolay, S. Schmidt, S. Hufner, R. Claessen, V. Eyert, and C. Geibel, Phys. Rev. B **64**, 235104 (2001).

[28] J. C. Fuggle, F. U. Hillebrecht, Z. Zolnierek, R. Lasser, C. Freiburg, O. Gunnarsson, and K. Schonhammer, Phys. Rev. B **27**, 7330 (1983); J. C. Fuggle, O. Gunnarsson, G. A. Sawatzky, and K. Schönhammer, *ibid.* **37**, 1103 (1988).

[29] T. Endstra, G. J. Nieuwenhuys, and J. A. Mydosh, Phys. Rev. B **48**, 9595 (1993).

[30] D. D. Sarma, N. Shanthi, S. R. Barman, N. Hamada, H. Sawada, and K. Terakura, Phys. Rev. Lett. **75**, 1126 (1995).

[31] A. Chakrabarti, C. Biswas, S. Banik, R. S. Dhaka, A. K. Shukla, and S. R. Barman, Phys. Rev. B **72**, 073103 (2005).